Physica E 91 (2017) 82–87

Contents lists available at ScienceDirect

Physica E

journal homepage: www.elsevier.com/locate/physe

Elastic, electronic and optical properties of stable pentagonal ZnO_2

Lu-Si Zhao[a,b], Ying Wang[a,b], Chun-Ping Chen[a,b], Lin-Lin Liu[a,b], Hong-Xia Yu[a,b], Yong Zhang[c], Yi Chen[a,b], Xiao-Chun Wang[a,b,*]

[a] Institute of Atomic and Molecular Physics, Jilin University, Changchun 130012, China
[b] Jilin Provincial Key Laboratory of Applied Atomic and Molecular Spectroscopy (Jilin University), Changchun, 130012, China
[c] Department of Electrical and Computer Engineering, The University of North Carolina at Charlotte, Charlotte, NC 28223-0001, USA

ARTICLE INFO

Keyword:
Penta-ZnO_2
Flexibility
First principles

ABSTRACT

Using first-principles calculations, we predict the existence of two dimensional (2D) pentagonal ZnO_2 (penta-ZnO_2) sheet and confirm that penta-ZnO_2 is dynamically and mechanically stable. Due to its unique atomic configuration, penta-ZnO_2 has intrinsic negative Possion's ratio, contrary to the most existing materials. Furthermore, Penta-ZnO_2 is much more flexible than graphene-like ZnO and penta-graphene in elasticity. Using the Heyd-Scuseria-Ernzerhof (HSE06) functional, the calculated indirect energy band gap is 4.53 eV, which is corresponding with optical gap (4.54 eV). More interesting, in the visible range of light, we find that penta-ZnO_2 has very low reflectance (0.0035%). Together with the expected zero absorption below the band gap, the light transmittance of penta-ZnO_2 is almost 100% in a broad spectral range. Our study demonstrates that penta-ZnO_2 possesses unique stable structure and promising mechanical, electronic and optical properties, which offers great potential in a wide range of applications in optoelectronics. Especially, the high flexibility and high light transmission make the penta-ZnO_2 to be a promising candidate for transparent electrodes.

1. Introduction

Metal oxides are a fascinating class of materials with diverse physical, chemical, and electronic properties [1]. Metal oxides are widely used in electronic and magnetic devices, heterogeneous catalysis, and other applications [2]. Among the metal oxides, zinc oxide (ZnO) has attracted extensive attention for half a century as a unique material because of its semiconducting and piezoelectric properties. Configurations of ZnO include hexagonal wurtzite and cubic zinc blende structures. ZnO with hexagonal wurtzite structure is the most thermodynamically stable and is thus the most commonly found form [3]. ZnO not only has a wide band gap (~3.37 eV) and a large excitation binding energy (~60 meV), but also possesses excellent piezoelectricity [4–6]. These unique properties lend it to a variety of applications such as in transparent electronics, ultraviolet (UV) light emitters, piezoelectric devices, chemical sensors, spin electronics, and catalysis [5]. The wurtzite ZnO can exist with a large number of morphologies such as nanotube, nanowires, nanobelts, nanorings, nanohelixes [3,7,8].

The advent of graphene, a two-dimensional (2D) honeycomb lattice of sp^2-bonded carbon atoms, and its extraordinary properties [9,10] has triggered the development of new classes of two-dimensional materials, particularly those with an intrinsic band gap. Graphene-like ZnO (g-ZnO) is one of them. Structurally, Zn atoms are located in the same plane as the O atoms. The bonding configuration of the Zn and O atoms in the ZnO layers changes from the sp^3 tetrahedral in the wurtzite structure to sp^2 trigonal coordination [11–13]. Consequently, the binding energy of g-ZnO is greatly less than that of the wurtzite structure [11]. Monolayer g-ZnO has a direct band gap of 3.37 eV, which is promising for switching electronics applications [3]. ZnO single layers are much more flexible than graphite single layers in elasticity and stronger than boron nitride single layers in piezoelectricity [7]. Very recently, the 2D metastable carbon allotrope, penta-graphene, composed entirely of carbon pentagons and resembling the Cairo pentagonal tiling, was proposed [14]. It is shown that while the unique pentagonal crystal symmetry provides a dynamical stability (for temperatures up to 1000 K), the buckled nature of the penta-graphene leads to a negative value for its Poisson's ratio. Furthermore, unlike graphene that needs to be functionalized for opening a band gap, penta-graphene possesses an intrinsic quasi-direct band gap as large as 3.25 eV, which is close to that of ZnO and GaN. Inspired by this study, B_2C [15], BN_2 [16], CN_2 [17], SiC_2 [18]and AlN_2 [19] with pentagonal lattices have also been reported. As far as we know, the two-dimensional pentagonal structure composed of zinc and oxygen elements has not been reported.

In this paper, we propose a 2D all-pentagon sheet with a chemical formula, ZnO_2. This new structure, termed as penta-ZnO_2, is composed

* Corresponding author at: Institute of Atomic and Molecular Physics, Jilin University, Changchun 130012, China.
E-mail address: wangxiaochun@jlu.edu.cn (X.-C. Wang).

http://dx.doi.org/10.1016/j.physe.2017.03.017
Received 10 January 2017; Received in revised form 21 February 2017; Accepted 22 March 2017
Available online 23 March 2017
1386-9477/

of three atomic layers, rather than the other 2D zinc oxide in which all atoms are in the same plane. Using first-principles density functional calculations, we present a comprehensive theoretical study on penta-ZnO_2. The calculated results confirm that penta-ZnO_2 is not only dynamically and mechanically stable, but also much more flexible than g-ZnO in elasticity. Penta-ZnO_2 also has an intrinsic negative Possion's ratio. Normally, for most materials including all the other compounds of oxygen and zinc, the Possion's ratio is positive. For penta-ZnO_2, the stoichiometry ratio Zn:O is 1:2, which is quite different from the ratio (1:1) of the previously known oxygen and zinc compound structures [7,20,21]. Penta-ZnO_2 intrinsically has a very high transmittance of light in the visible range. The flexible display requires flexible structure and high transmittance in the visible range of light. The research results will show that the penta-ZnO_2 can be used for all cases transparent conducting layers are required, ranging from display, PV, LED, detector, etc.

2. Computational details

Atomic structure optimizations and electronic structure calculations are carried out using density functional theory (DFT) as implemented in the Vienna ab initio Simulation Package(VASP) [22]. Projector augmented wave (PAW) [23] method is used to treat the core electrons. Plane waves with a kinetic energy cutoff of 600 eV are used to expand the valance electron ($3d^{10}4s^2$ for Zn, and $2s^22p^4$ for O) wavefunctions. Perdew–Burke–Ernzerhof (PBE) exchange-correlation functional within generalized gradient approximation(GGA) [24] and Heyd-Scuseria-Ernzerhof (HSE06) [25,26] functional are used. The 2D system is separated from its periodic images by a vacuum distance of 20 Å in the perpendicular direction to avoid virtual interactions. The tetrahedron method with the Blöchl corrections [27] give a good account for electronic density of states (DOS). The first Brillouin zone is sampled by a 14×14×1 k-point grid within the Monkhorst–Pack scheme [28] for the primitive unit cells in most of our calculations. We have tested the total energy convergence to be within 0.01% difference with respect to the number of k points. For geometry relaxation, the convergence thresholds for total energy and atomic force components are set at 10^{-5} eV and 10^{-3} eV $Å^{-1}$, respectively. To check the dynamic stability, phonon properties are calculated using finite displacement method implemented using the supercell method through the PHONOPY code [29] and a (4×4) supercell is constructed to calculate the atomic forces by using VASP.

3. Results and discussion

3.1. Structural properties

The optimized 2D pentagonal crystal structure of ZnO_2 possesses P-42_1m symmetry (space group no. 113) with a tetragonal lattice as shown in Fig. 1. The optimize lattice constants are a = b = 4.49 Å. The relaxed structure of penta-ZnO_2 is composed of three atomic layers with Zn atoms in the middle layer and O atoms on the top and bottom layers, which is different from g-ZnO where Zn and O atoms are located in the same plane. The unit cell contains four oxygen atoms and two zinc atoms, which is denoted by black dashed lines in Fig. 1. Each zinc atom highlighted in gray is 4-coordinated with four oxygen atoms highlighted in red. In the unit cell of penta-ZnO_2, the ratio of the number of atoms between Zn and O is 1:2, which is quite different from the 1:1 ratio of the most previously known oxygen and zinc compound structures, such as wurtzite and graphene-like ZnO structures [3]. From the side view, a buckling of h=0.8 Å is observed, leading to a 2D sheet with a total thickness of 1.60 Å, which is larger than that of penta-graphene (1.20 Å) [14]. The "thickness" of this sheet is defined as the vertical coordinate difference between the oxygen atoms in the top and bottom layers, which is expected to be significantly smaller than that if it would be measured by AFM. The Zn–O and O–O bond lengths are 1.984 Å and 1.497 Å respectively. The bond angle of $\theta_{O\text{-}Zn\text{-}O}$, $\theta_{Zn\text{-}O\text{-}Zn}$, and $\theta_{Zn\text{-}O\text{-}O}$ are 100.3°, 106.4°, and 115.1° respectively. The specific binding energy E_b was calculated using the formula$E_b=(E_t-\sum n_aE_a)/\sum n_a$, where E_a denotes the energy of a single isolated atom and n_a denotes the number of atoms of one particular type in the unit cell. E_t is the total energy of the unit cell. The specific binding energy of penta-ZnO_2 is -4.203 eV/atom, lower than -4.123 eV/atom of g-ZnO and higher than -4.473 eV/atom of wurtzite ZnO [7].

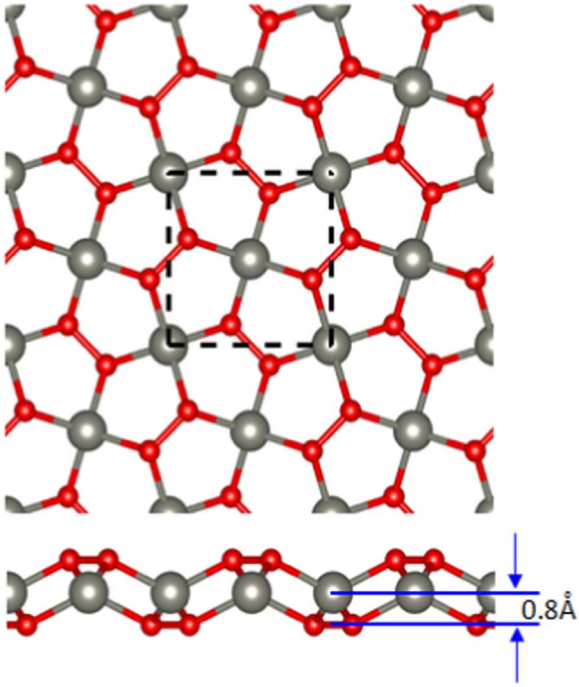

Fig. 1. Top and side views of optimized structure of penta-ZnO_2. Gray and red spheres represent zinc and oxygen atoms, respectively. The square marked by black dashed lines denotes a unit cell. (For interpretation of the references to color in this figure legend, the reader is referred to the web version of this article.)

3.2. Phonon dispersion and thermodynamic properties

Next we study the dynamical stability of penta-ZnO_2 by calculating its phonon dispersion. The unit cell of penta-ZnO_2 has six atoms, suggesting that there are 18 modes for any one q vector or 18 dispersion curves. The results are presented in Fig. 2(a). There is no imaginary frequencies in the entire Brillouin zone, which confirms that penta-ZnO_2 is dynamically stable. The two highest optical modes are separated from others by a large phonon gap of around 8 THz. The vibration modes below 5 THz including the three acoustic bands and three optical bands are mainly contributed by Zn due to its larger atomic mass [30]. Detailed analysis of the atom-resolved phonon density of states (PhDOS) reveals that the bonds between the O atoms are predominant in the dispersionless high-frequency modes shown in the right pattern of Fig. 2(a).

Based on the calculated phonon spectrum, a series of thermodynamic properties can be derived in terms of the harmonic approximation. The free energy $F(T)$, entropy $S(T)$ and heat capacity at constant volume $C_v(T)$ are given by applying the following formula [31,32]:

$$F(T) = E_{tot}+E_{zp}+k_BT\int F(\omega)\ln\{1-\exp[-h\omega/(k_BT)]\}d\omega \quad (1)$$

$$S(T) = k_B\left\{\int \frac{h\omega/k_BT}{\exp[h\omega/(k_BT)]-1}F(\omega)d\omega - \int F(\omega)\ln\left\{1-\exp\left[-\frac{h\omega}{k_BT}\right]\right\}d\omega\right\} \quad (2)$$

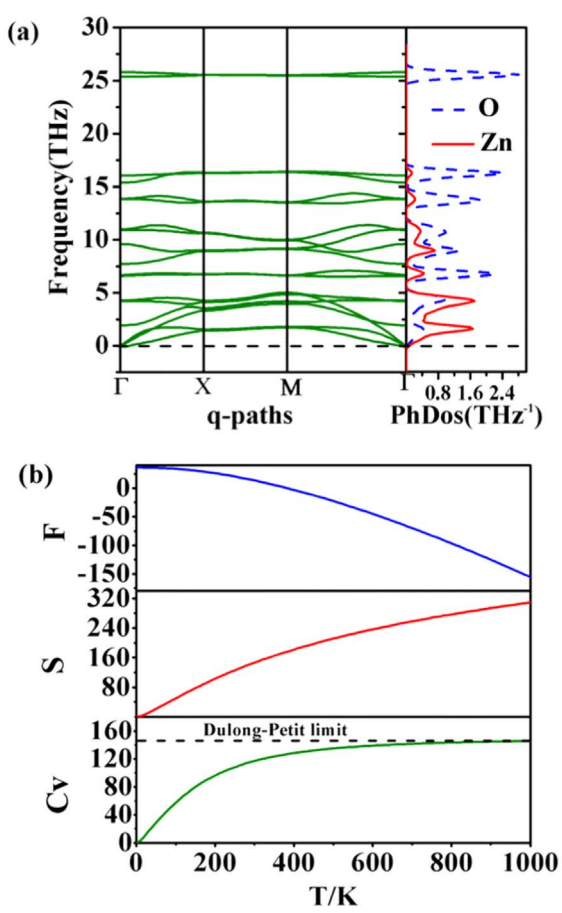

Fig. 2. (a) Phonon spectrum and PhDOS of penta-ZnO_2 . High-symmetric q-point paths is Γ (0, 0, 0)→X (1/2, 0, 0)→M (1/2, 1/2, 0)→Γ (0, 0, 0) of Brillouin zone. (b) Thermodynamic properties: Free energy (F), entropy (S) and heat capacity (C_V) for penta-ZnO_2.

$$C_v(T) = k\int \frac{(k\omega/kT)^2 \exp(h\omega/kT)}{\exp(h\omega/kT)-1} F(\omega)d\omega \quad (3)$$

where E_{tot} is the total energy, E_{zp} is the zero point energy, h is the Planck's constant, $F(\omega)$ is the phonon density of states and T is temperature. In this work, the free energy (F) is equal to the Gibbs free energy (G) because the calculations were carried out under 0 GPa. Fig. 2(b) show the temperature-dependent free energy (F), entropy (S) and heat capacity at constant volume (C_υ) of penta-ZnO_2. Both entropy (S) and heat capacity (C_υ) increase with the increasing temperature, but free energy (F) exhibits a reverse trend. As the temperature increases from 0 K to 1000 K, the entropy (S) increases from 0 J mol^{-1} K^{-1} to 309.23 J mol^{-1} K^{-1}, but free energy (F) decreases from 36.14 kJ mol^{-1} to -155.25 kJ mol^{-1}. The smaller the Gibbs free energy is, the better the thermal stability of compounds is. Hence, the calculated Gibbs free energies show that the thermal stability of penta-ZnO_2. When the temperature is about 400 K, the free energy is equal to zero. When the temperature is higher than 400 K, it is less than zero, which suggests that penta-ZnO_2 may be stable. For the heat capacity (C_υ), with increasing temperature, it increases sharply and is proportional to T^3 at lower temperature, which exhibits strong dependence on temperature when temperature is less than 400 K. Then the heat capacity (C_υ) increases slowly in the higher temperature region and tend to the Dulong–Petit limit (145.47 J mol^{-1} K^{-1}). It indicates that the interactions between Zn and O atoms primarily occur in the low temperature region.

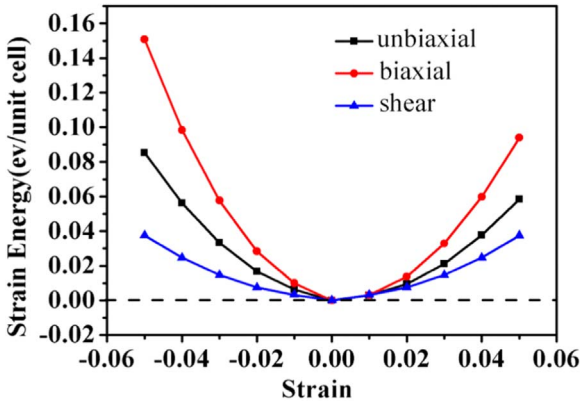

Fig. 3. Strain energy of penta-ZnO_2 under different kinds of in-plane strain.

3.3. Mechanical stability and elastic properties

We calculate the elastic constants in order to explore how lattice distortions affect the structural stability of penta-ZnO_2, and to examine its mechanical stability. The elastic constants can be derived by fitting the energy curves associated with uniaxial, biaxial and shear strains. These curves are plotted in Fig. 3. After fitting, the 2D coefficient C_{ij}^{2D} must be renormalized by the z lattice parameter corresponding to the spacing between 2D layers [33]. Thus, the elastic constant calculation shows C_{11}=C_{22}=44.79 GPa nm. C_{12} and C_{66} are obtained to be -6.38 GPa nm and 5.74 GPa nm, respectively. The absolute values of these elastic constants are much smaller than that of 265 GPa nm, -18 GPa·nm and 37.82 GPa nm for penta-graphene respectively [14]. In other words, the stiffness of penta-ZnO_2 is smaller than that of penta-graphene, and penta-ZnO_2 is more prone to deformation. Obviously, these elastic constants satisfy Born-Huang criteria [34,35], namely, $C_{11}C_{22}$-$C_{12}^2 > 0$ and $C_{66} > 0$, indicating that penta-ZnO_2 is mechanically stable. Based on the obtained elastic constants [36], the in-plane Young's modulus E and Poisson's ratio ν can be calculated using E=(C_{11}^2-C_{12}^2)/C_{11} and ν_{12}=ν_{21}=C_{12}/C_{11} respectively. The in-plane Young's modulus of penta-ZnO_2 is 43.88 GPa nm, which is less than 1/2 times of g-ZnO (101.2 GPa nm) and 1/6 times of penta-graphene (263.8 GPa nm) [7,14]. The lower value the Young's modulus of material is, the more flexible the material is. Therefore, penta-ZnO_2 is much more flexible than penta-graphene and g-ZnO in elasticity along x axis and y axis directions in the 2D material plane. More interestingly, the value ν_{12}=ν_{21}=-0.14 indicates a negative Possion's ratio, contrary to the positive values found for most existing materials including all the other compounds of oxygen and zinc. The magnitude of this negative Possion's ratio is much larger than -0.068 for penta-graphene by about a factor of 2 [14]. This fact means when this material is stretched, it expands transversely in the elastic range much easier than penta-graphene. Normally, a material with a positive Possion's ratio shrinks in the transverse direction when subjected to a uniaxial expansion. Nearly all auxetic materials whose microstructures have been specifically engineered to generate a negative Poisson's ratio are bulk materials [37]. In contrast to structure-engineered bulk auxetics, the negative Poisson's ratio is intrinsic in the penta-ZnO_2 sheet.

3.4. Electronic properties

To study the electronic properties of penta-ZnO_2, we calculate its band structure and corresponding total density of states (TDOS) and partial density of states (PDOS), using the Heyd-Scuseria-Ernzerh (HSE06) [25,26] functional, as shown in Fig. 4(a). The valance band maximum (VBM) and the conduction band minimum (CBM) are located on the M-Γ

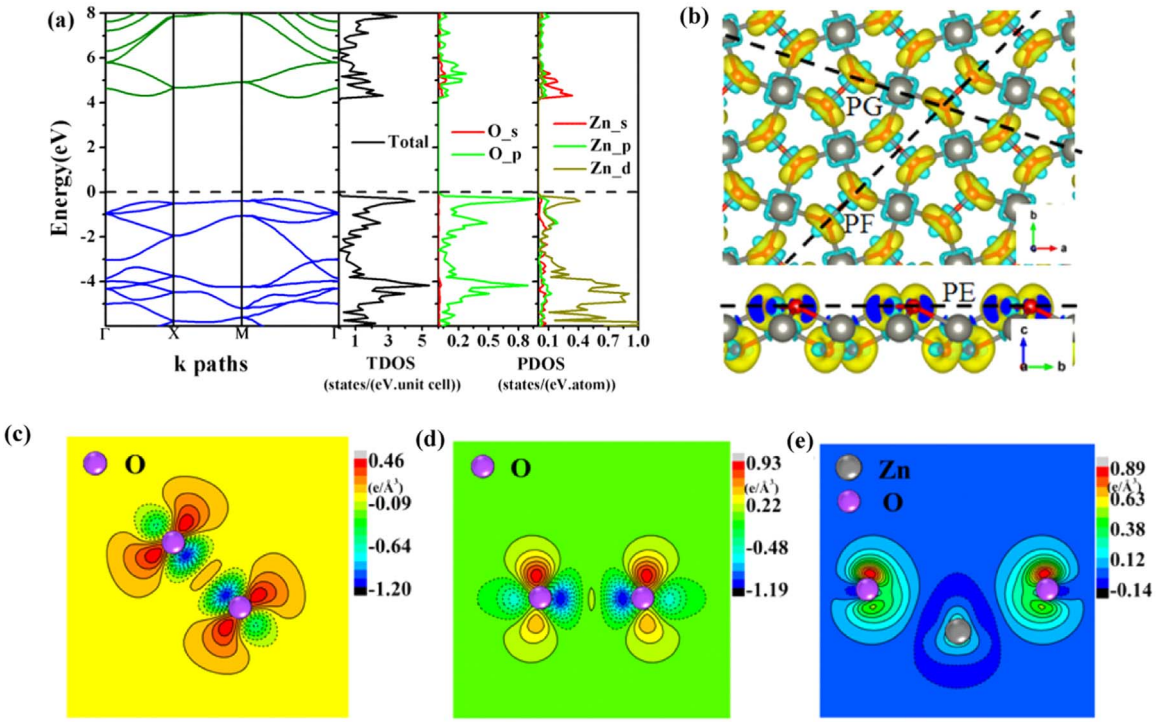

Fig. 4. (a) Electronic band structure, total density of states (TDOS) and partial density of states (PDOS) of penta-ZnO_2. The Fermi level is shifted to 0.00 eV. (b) Three dimensional (3D) plots of charge density difference of penta-ZnO_2 (up and down patterns are for top and side views respectively). (c–e) are 2D plots of charge density difference of penta-ZnO_2. The planes of (c–e) are along the dashed lines PE, PF and PG in (b) respectively and perpendicular to the plane of the paper.

path, but at slightly different k points: (0.217, 0.217, 0) for CBM, and (0.333, 0.333, 0) for VBM. Thus, penta-ZnO_2 is an indirect band-gap semiconductor with a band gap of 4.53 eV. However, because the VBM dispersion is rather small, about 91 meV below the VBM, at the same k point of the CBM, penta-ZnO_2 could be regarded as a quasi-direct band-gap semiconductor. The band gap is larger than that of wurtzite ZnO material (3.37 eV) [3]. In the TDOS, there is a very high peak above the Fermi level and the corresponding energy value is about 4.3 eV, which is consistent with band structure. The calculated PDOS suggests that the highest occupied band are mainly dominated by O-2p states, while the lowest unoccupied band are mainly contributed by Zn-4s states.

In order to understand the chemical bonding of penta-ZnO_2, we computed the charge density difference of penta-ZnO_2, which is defined as the total charge density with the contribution of isolated Zn and O atoms being subtracted. In the 3D charge density difference plots (Fig. 4(b)), yellow and blue refer to regions of electron accumulation and depletion, respectively. The dashed line PE crosses the first oxygen atoms layer of the penta-ZnO_2 sheet, and the dashed line PF crosses the neighboring O atoms, and the dashed line PG crosses the neighboring O and Zn atoms. Fig. 4(c–e) are 2D plots of charge density difference of penta-ZnO_2. A positive value (solid contour line) indicates an increase in electron density and a negative value (dashed contour line) means the electron density loss with respect to the superposition of the atomic electron density. The planes of Fig. 4(c–e) are along the dashed lines PE, PF and PG in Fig. 4(d) respectively and perpendicular to the plane of Fig. 4(b). The plotted plane of Fig. 4(c) is parallel to the penta-ZnO_2 sheet and crosses the neighboring O atoms to show the charge transfer of the neighboring O atoms. Fig. 4(c) shows that there is electronic charge accumulation in the middle of the bond between the neighboring O atoms, which indicates that the O-O covalent-like bonds are formed. There is obviously electronic charge accumulation region that is around O atom and vertical with the O-O bond, which indicates the antibonding state property. The plotted plane of Fig. 4(d) crosses the neighboring O atoms as well, but it is perpendicular to the penta-ZnO_2 sheet. Fig. 4(d) indicates there is also an antibonding state electronic charge around O atoms. Moreover, according to Fig. 4(c) and (d), there are areas of electronic charge accumulation around the neighboring O atoms, which indicates that the π-like bond between the neighboring O atoms are formed, besides the O-O covalent-like bonds. The plotted plane of Fig. 4(e) crosses the neighboring O and Zn atoms to visualize the characteristics of bonding between them. There is electronic charge depletion around the Zn atoms and the electronic charge is obviously accumulated near O atoms. Thus, there are certain electronic charge transfers from Zn atoms to O atoms. The bond between Zn and O atoms shows the ionic bond property.

3.5. Optical properties

In this section, the linear optical properties of penta-ZnO_2 are derived from its reliable electronic structures using HSE06 method. The optical properties of a material is described by the dielectric function $\varepsilon(\omega)$ as a function of the frequency or the wavelength. It consists of two parts $\varepsilon_1(\omega)$ and $\varepsilon_2(\omega)$.

$$\varepsilon(\omega) = \varepsilon_1(\omega) + i\varepsilon_2(\omega) \tag{4}$$

The imaginary part $\varepsilon_2(\omega)$ is expressed as [38]

$$\varepsilon_2(\omega) = \frac{4}{\pi\omega^2}\sum_{nn'}\int |P_{nn'}(k)|^2 \frac{dS_k}{\nabla\omega_{nn'}(k)} \tag{5}$$

The real part $\varepsilon_1(\omega)$of the dielectric function can be calculated from the imaginary part $\varepsilon_2(\omega)$ by Kramer–Kronig relationship [38]

$$\varepsilon_1(\omega) = 1 + \frac{2}{\pi}P\int_0^{\infty} \frac{\omega'\varepsilon_2(\omega')}{\omega'^2 - \omega^2} d\omega' \tag{6}$$

All optical properties are obtained from the dielectric function [39]. The absorption coefficient $I(\omega)$:

$$I(\omega) = \sqrt{2}\,(\omega)\left(\sqrt{\varepsilon_1(\omega)^2 + \varepsilon_2(\omega)^2} - \varepsilon_1(\omega)\right)^{1/2} \tag{7}$$

The reflectivity $R(\omega)$:

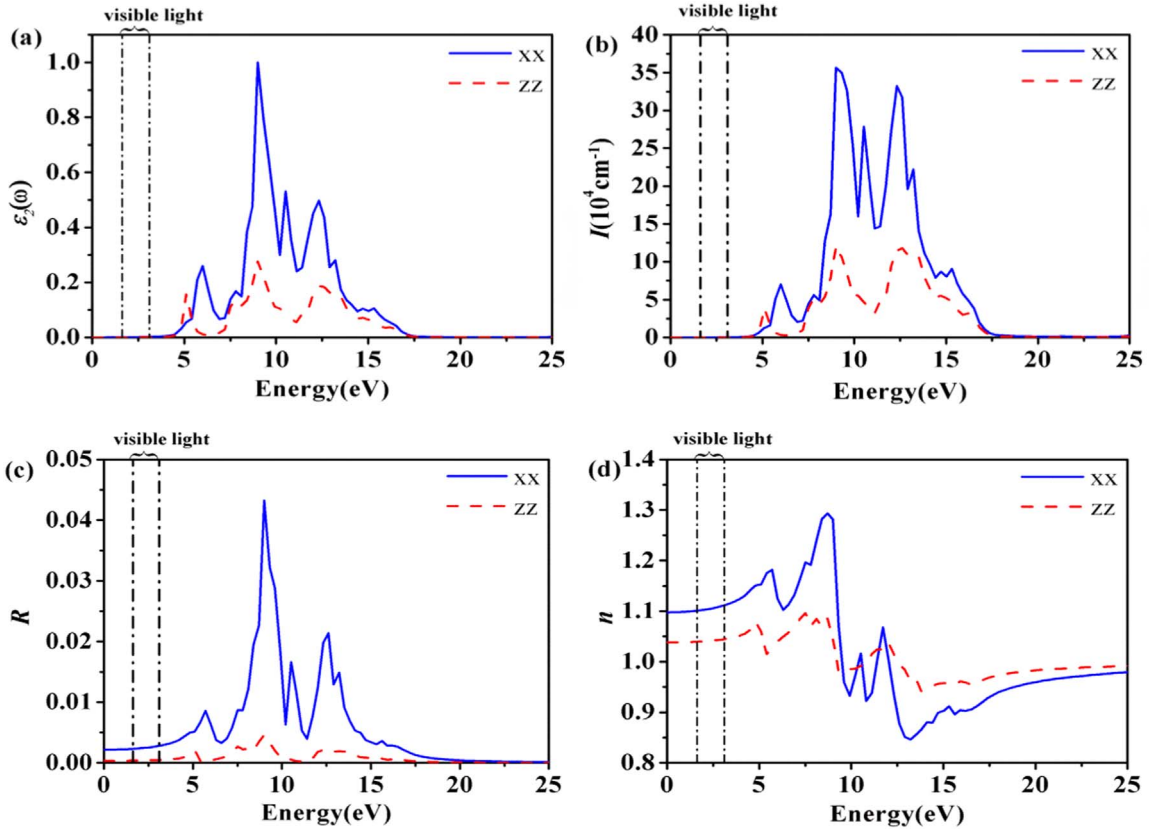

Fig. 5. (a) the imaginary part of the dielectric function $\varepsilon_2(\omega)$, (b) the absorption coefficient I, (c) the reflectivity R and (d) the refraction index n of penta-ZnO_2.

$$R(\omega) = \left|\frac{\varepsilon^{1/2}(\omega)-1}{\varepsilon^{1/2}(\omega)+1}\right|^2 \quad (8)$$

The refraction index $n(\omega)$:

$$n(\omega) = \left[\frac{\sqrt{\varepsilon_1(\omega)^2+\varepsilon_2(\omega)^2}}{2} + \frac{\varepsilon_1(\omega)}{2}\right]^{1/2} \quad (9)$$

Because of the symmetry of penta-ZnO_2, these optical properties in xx direction are identic with those in yy direction. Then we only show the optical properties in xx and zz directions in Fig. 5, although the xx and yy directions are more meaningful than zz direction for a 2D material. The imaginary part of the dielectric function allows to deduce the optical transition between the conduction and valence band as presented in Fig. 5(a). In xx (yy) and zz directions, the edge of the imaginary part corresponds to the first transition occurring at 4.54 eV (or 273 nm wavelength), corresponding to the band gap energy. It can be attributed to the transition between O-2p states located at the top of the valance band and Zn-4s states located at the conduction band minimum according to the PDOS. The energy level corresponding to the threshold of the imaginary part of penta-ZnO_2 locates much higher than that of wurtzite ZnO (2.8 eV) [38] and g-ZnO (3.58 eV) [40]. Fig. 5(b) shows the absorption coefficient spectra of penta-ZnO_2. These absorption peaks in Fig. 5(b) is consistent with the imaginary part of penta-ZnO_2. Penta-ZnO_2 does not absorb visible light within the energy range from 1.62 eV to 3.11 eV according to our calculated results and has no absorption even in the near UV region of light. It is clearly shown that the optical absorption edge of penta-ZnO_2 shifts to higher energy compared with wurtzite ZnO [38] and g-ZnO [41]. Namely, penta-ZnO_2 allows the extension of the absorption edge towards shorter wavelength. This shift of the absorption edge can be related to the increase of the energy band gap. The reflectivity R presented in Fig. 5(c) is also an important optical property. In xx (yy) direction, it shows that a weak reflectivity of less than 0.25% in the visible spectral range of light. In zz direction, the calculated reflectivity of penta-ZnO_2 is 0.0035%, which is much lower than that of wurtzite ZnO [38] and g-ZnO [41]. The reflectivity of penta-ZnO_2 begins to rise steeply at about 5 eV. In xx direction, zero absorption and extremely small reflectivity enable us to deduce that the light transmittance of penta-ZnO_2 is almost 100%, higher than the wurtzite ZnO (75%-85%) [38] and the doped g-ZnO (> 90%) [42]. The refraction index denoted by n in Fig. 5(d) is characteristic property which also helps us to describe the behavior of light in the materials. In xx (yy) and zz directions, the refraction index of penta-ZnO_2 remains at 1.10 and 1.04 in the visible range of light respectively, and begins to increase until the energy reaches around 5 eV. This fact allows the visible light transmit the penta-ZnO_2 sheet maintaining the almost same direction for any direction of incidence.

4. Conclusion

In this study, we investigated theoretically the stability, mechanical, electronic and optical properties of penta-ZnO_2. Our calculations demonstrate that penta-ZnO_2 has buckled geometry. The structure is composed of three atomic layers with Zn atoms in the middle layer and O atoms on the top and bottom layers, rather than a single planar layer structure of g-ZnO. Penta-ZnO_2 is not only dynamically stable because of no imaginary frequencies in the phonon spectrum, but also mechanically stable because the calculated elastic constants satisfy Born-Huang criteria. Penta-ZnO_2 is a semiconductor with an indirect band gap of 4.53 eV, which is larger than penta-graphene and previous ZnO materials. Especially, Penta-ZnO_2 has intrinsic negative Possion's ratio and is much more flexible than g-ZnO and penta-graphene in elasticity. In the visible range of light, penta-ZnO_2 has zero absorption, 0.0035% reflectivity and 1.04 refraction index in zz direction. It is deduced that penta-ZnO_2 itself can possess very high transparency in the visible ranges of light. In summary, penta-ZnO_2 possesses unique stable structure and promising mechanical, electronic

and optical properties, which gives the penta-ZnO_2 sheet many potential applications in optoelectronic devices. It is worth mentioning that the high flexibility and the high transmission of visible light make the penta-ZnO_2 to be a promising candidate to be used in flexible devices for display and detector, etc.

Acknowledgments

This work was supported by the National Natural Science Foundation of China (Grant no. 11474123), and the Natural Science Foundation of Jilin Province of China (Grant no. 20170101154JC). YZ thanks the support of Bissell Distinguished Professorship at UNC-Charlotte.

References

[1] P. Cox, The Surface Science of Metal Oxides, Cambridge university press, Cambridge, 1996.
[2] A. Umar, Y.-B. Hahn, Metal Oxide Nanostructures and their Applications, American Scientific Publ, USA, 2010.
[3] H.T. Quang, A. Bachmatiuk, A. Dianat, F. Ortmann, J. Zhao, J.H. Warner, J. Eckert, G. Cunniberti, M.H. Rummeli, In situ observations of free-standing graphene-like mono- and bilayer ZnO membranes, ACS Nano 9 (2015) 11408–11413.
[4] Z.L. Wang, Towards self-powered nanosystems: from nanogenerators to nanopiezotronics, Adv. Funct. Mater. 18 (2008) 3553–3567.
[5] Z.L. Wang, Zinc oxide nanostructures: growth, properties and applications, J. Phys.: Condens. Matter 16 (2004) R829.
[6] J.W. Wang, Y. Zhang, L.W. Wang, Systematic approach for simultaneously correcting the band-gap and p-d separation errors of common cation III–V or II–VI binaries in density functional theory calculations within a local density approximation, Phys. Rev. B 92 (2015) 10.
[7] Z. Tu, X. Hu, Elasticity and piezoelectricity of zinc oxide crystals, single layers, and possible single-walled nanotubes, Phys. Rev. B 74 (2006) 035434.
[8] Q. Tang, Y.F. Li, Z. Zhou, Y.S. Chen, Z.F. Chen, Tuning electronic and magnetic properties of wurtzite ZnO nanosheets by surface hydrogenation, ACS Appl. Mater. Interfaces 2 (2010) 2442–2447.
[9] J.H. Warner, F. Schaffel, M. Rummeli, A. Bachmatiuk, Graphene: Fundamentals and Emergent Applications, Newnes, Holland, 2012.
[10] V.I. Fal'ko, Introducing 2D Materials-a new multidisciplinary journal devoted to all aspects of graphene and related two-dimensional materials, 2D Materials 1 (2014) 3.
[11] E. Kan, K. Deng, F. Wu, Stability of graphitic-like zinc oxide layers under carriers doping: a first-principles study, Nanoscale 5 (2013) 12111–12114.
[12] J. Lee, D.C. Sorescu, X. Deng, Tunable lattice constant and band gap of single-and few-layer ZnO, J. Phys. Chem. Lett. 7 (2016) 1335–1340.
[13] W. Song, K.W. Kim, S.J. Kim, B.K. Min, Y.R. Lim, S. Myung, S.S. Lee, J. Lim, K.S. An, Threshold voltage manipulation of ZnO-graphene oxide hybrid thin film transistors via Au nanoparticles doping, 2D Materials 2 (2015) 5.
[14] S. Zhang, J. Zhou, Q. Wang, X. Chen, Y. Kawazoe, P. Jena, Penta-graphene: a new carbon allotrope, Proc. Natl. Acad. Sci. 112 (2015) 2372–2377.
[15] F.Y. Li, K.X. Tu, H.J. Zhang, Z.F. Chen, Flexible structural and electronic properties of a pentagonal B2C monolayer via external strain: a computational investigation, Phys. Chem. Chem. Phys. 17 (2015) 24151–24156.
[16] M. Yagmurcukardes, H. Sahin, J. Kang, E. Torun, F.M. Peeters, R.T. Senger, Pentagonal monolayer crystals of carbon, boron nitride, and silver azide, J. Appl. Phys. 118 (2015).
[17] S. Zhang, J. Zhou, Q. Wang, P. Jena, Beyond graphitic carbon nitride: nitrogen-rich penta-CN2 sheet, J. Phys. Chem. C 120 (2016) 3993–3998.
[18] A. Lopez-Bezanilla, P.B. Littlewood, Sigma-pi-band inversion in a novel two-dimensional material, J. Phys. Chem. C 119 (2015) 19469–19474.
[19] J. Li, X. Fan, Y. Wei, H. Liu, S. Li, P. Zhao, G. Chen, Half-metallicity and ferromagnetism in penta-AlN2 nanostructure, Sci. Rep. 6 (2016).
[20] J. Wang, Y. Zhang, L.-W. Wang, Systematic approach for simultaneously correcting the band-gap andp−dseparation errors of common cation III–V or II–VI binaries in density functional theory calculations within a local density approximation, Phys. Rev. B 92 (2015).
[21] J. Wang, Y. Zhang, Topologic connection between 2-D layered structures and 3-D diamond structures for conventional semiconductors, Sci. Rep. 6 (2016) 24660.
[22] G. Kresse, J. Furthmüller, Efficient iterative schemes for ab initio total-energy calculations using a plane-wave basis set, Phys. Rev. B 54 (1996) 11169.
[23] P.E. Blöchl, Projector augmented-wave method, Phys. Rev. B 50 (1994) 17953.
[24] J.P. Perdew, K. Burke, M. Ernzerhof, Generalized gradient approximation made simple, Phys. Rev. Lett. 77 (1996) 3865.
[25] J. Heyd, G.E. Scuseria, M. Ernzerhof, Hybrid functionals based on a screened Coulomb potential, J. Chem. Phys. 118 (2003) 8207–8215.
[26] J. Heyd, G.E. Scuseria, M. Ernzerhof, Hybrid functionals based on a screened Coulomb potential, J. Chem. Phys. 124 (2006) 1 (vol 118, pg 8207, 2003).
[27] P.E. Blöchl, O. Jepsen, O.K. Andersen, Improved tetrahedron method for Brillouin-zone integrations, Phys. Rev. B 49 (1994) 16223.
[28] H.J. Monkhorst, J.D. Pack, Special points for Brillouin-zone integrations, Phys. Rev. B 13 (1976) 5188.
[29] A. Togo, F. Oba, I. Tanaka, First-principles calculations of the ferroelastic transition between rutile-type and CaCl 2-type SiO_2 at high pressures, Phys. Rev. B 78 (2008) 134106.
[30] W. Li, N. Mingo, Lattice dynamics and thermal conductivity of skutterudites CoSb 3 and IrSb 3 from first principles: Why $IrSb_3$ is a better thermal conductor than $CoSb_3$, Phys. Rev. B 90 (2014) 094302.
[31] F. Wang, S.-j Sun, B. Yu, F. Zhang, P.-l Mao, Z. Liu, First principles investigation of binary intermetallics in Mg-Al-Ca-Sn alloy: Stability, electronic structures, elastic properties and thermodynamic properties, Trans. Nonferr. Met. Soc. 26 (2016) 203–212.
[32] B. Huang, Y.-H. Duan, Y. Sun, M.-J. Peng, S. Chen, Electronic structures, mechanical and thermodynamic properties of cubic alkaline-earth hexaborides from first principles calculations, J. Alloy. Compd. 635 (2015) 213–224.
[33] M.N. Blonsky, H.L. Zhuang, A.K. Singh, R.G. Hennig, Ab initio prediction of piezoelectricity in two-dimensional materials, ACS Nano 9 (2015) 9885–9891.
[34] M. Born, K. Huang, Dynamical Theory of Crystal Lattices, Clarendon Press, Oxford, 1954.
[35] J. Wang, S. Yip, S. Phillpot, D. Wolf, Crystal instabilities at finite strain, Phys. Rev. Lett. 71 (1993) 4182.
[36] K. Michel, B. Verberck, Theory of elastic and piezoelectric effects in two-dimensional hexagonal boron nitride, Phys. Rev. B 80 (2009) 224301.
[37] J.-W. Jiang, H.S. Park, Negative poisson's ratio in single-layer black phosphorus, Nat. Commun. 5 (2014).
[38] M. Khuili, N. Fazouan, H.A. El Makarim, G. El Halani, E.H. Atmani, Comparative first principles study of ZnO doped with group III elements, Jo. Alloy. Compd. 688 (2016) 368–375.
[39] X. Chen, Q.-Q. Zhao, X.-C. Wang, J. Chen, X. Ju, Linear optical properties of defective KDP with oxygen vacancy: First-principles calculations, Chin. Phys. B 24 (2015).
[40] Z. Tu, First-principles study on physical properties of a single ZnO monolayer with graphene-like structure, J. Comput. Theor. Nanosci. 7 (2010) 1182–1186.
[41] C.L. Tan, D. Sun, D.S. Xu, X.H. Tian, Y.W. Huang, Tuning electronic structure and optical properties of ZnO monolayer by Cd doping, Ceram. Int. 42 (2016) 10997–11002.
[42] Y. Kim, S.Z. Karazhanov, W. Kim, Influence of hydrogen on electrical and optical properties of ZnO films, Phys. Status Solidi (B) 248 (2011) 1702–1707.